# MODEL PREDICTIVE CONTROL FOR INDUSTRIAL DRIVE APPLICATIONS



Galina Mirzaeva
Senior Member, IEEE
The University of Newcastle
Callaghan, NSW2308
Australia
galina.mirzaeva@newcastle.edu.au

Yunxun Mo
PhD student
The University of Newcastle
Callaghan, NSW2308
Australia
yunxun.mo@uon.edu.au

***Abstract*** – Over the last two decades, Model Predictive Control (MPC) has gained popularity in the published research on power electronics. It is argued in the literature that MPC is well-suited for industrial variable speed drive (VSD) applications, due to its flexible and multi-objective nature. However, the adoption of MPC by industry has been slow. This paper reviews the VSD control strategies currently accepted by industry. It formulates expectations and determines the existing barriers for using MPC in VSD applications. The paper proposes a number of modifications to enhance the MPC performance and to offer new benefits to industry, compared to the existing solutions. The results of the paper are supported by simulations and validated by experiment.

*Index Terms* — AC motor drives, AC drive control, predictive control, common mode voltage, mining industry

## I. INTRODUCTION

Model predictive control (MPC) was introduced in the 1970s and was adopted in many industries, including chemical, automotive, etc. [1]. The advantages of MPC include time-domain formulation, flexibility and multi-objective nature, suitability for multiple-input multiple-output systems, easy handling of constraints and non-linearities. Application of MPC to power electronic converters was enabled by availability of powerful real-time processors in the early 2000s [2].

Since then MPC (particularly, its finite control set version, or FCS-MPC) has gained a growing popularity in the power electronics research community. FCS-MPC has been applied to different power converters, including 2-level inverter [3], multilevel inverter [4], matrix converter [5], and other topologies. However, the adoption of MPC-based power electronics solutions by industry has been very slow. The existing applications [6]-[7] utilize MPC for auxiliary functions while the main control schemes are still based on the traditional principles.

A variable speed drive (VSD) is one of the most challenging industrial applications of power electronic converters and their control. VSDs range from extra-low to high voltage levels. They need to provide good tracking performance, fast dynamic response and low harmonic distortion. Moreover, they must tolerate various disturbances and uncertainties of industrial environment. Two VSD control strategies that are widely used in industry for over 20 years are Field Oriented Control (FOC) [8] and Direct Torque Control (DTC) [9]-[10].

The current paper reviews the fundamental principles, the main features and the success factors of FOC and DTC. It provides valuable insights that help identify the existing shortcomings of MPC that currently prevent its acceptance by the industry.

Based on that, the paper proposes a number of important modifications to the conventional MPC scheme, leading to significant improvements of their performance. It is argued in the paper that, with the proposed enhancements in place, MPC can be competitive, or even superior, to the existing control strategies. Considering new developments in power electronic drive technologies, MPC is well positioned to become the first choice for future industry applications.

The remainder of the paper is organized as follows. Section II discusses the existing control strategies in AC drive applications, and their success factors. The MPC schemes known from the literature, are described in Section III. Section IV formulates performance expectations for a modern VSD and explains how these expectations can be met under the MPC strategy. Section V illustrates the proposed improvements using a specific VSD topology as a case study and validates the ideas by simulation and experiment. Conclusions of the paper are presented in Section VI, references - in Section VII, and the authors' vitae - in Section VII.

## II. THE EXISTING CONTROL SCHEMES FOR AC DRIVES

A structure of a general VSD is shown in Fig.1. When operating in *Speed control* mode, an external speed reference ($\omega_m^*$) is used by a closed-loop speed control (typically, of PID type) to generate a torque reference ($T^*$) for the *Inner loop control*. When operating in *Torque control* mode, the *Inner loop control* is driven directly by an external torque reference ($T_{em}^*$). The essential differences between various control schemes occur at the *Inner loop control* level.

Discussion in this paper is limited to vector control drive schemes. MPC, which is the main focus of the paper, also fits in this group. Vector control treats AC quantities as vectors (described by magnitude and phase) rather than scalars (described by magnitude only). Low-cost scalar control drives (also known as Constant Volt per Hz) are outside the scope of the current paper.

Vector control schemes commonly utilize space-vector representations of AC quantities. For balanced three-phase currents ($i_a, i_b, i_c$) the corresponding space vector is defined as

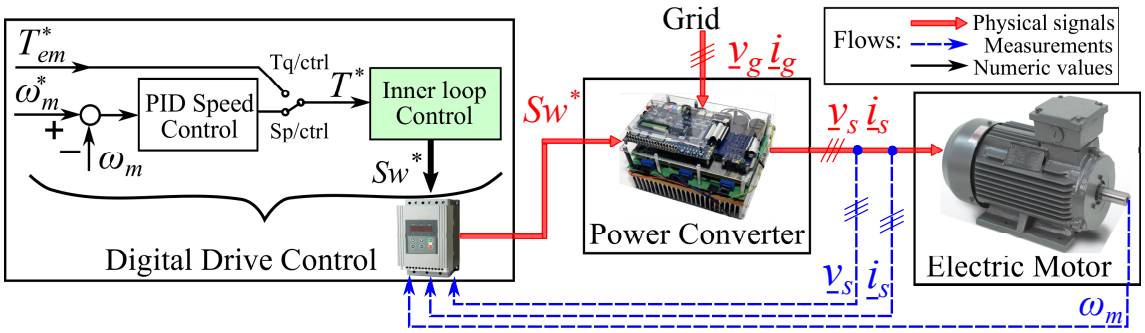


Fig. 1 General structure of a Variable Speed Drive

$$\vec{\imath} \triangleq \frac{2}{3}\left(i_a + i_b e^{j\frac{2\pi}{3}} + i_c e^{j\frac{4\pi}{3}}\right) \tag{1}$$

Its projections onto the axes of an orthogonal stationary frame $(\alpha\beta)$ and a rotating frame $(dq)$ can be determined using Clarke transform and Park transform, respectively, as follows:

$$\begin{bmatrix} i_\alpha \\ i_\beta \end{bmatrix} = \frac{2}{3}\mathbf{C}\begin{bmatrix} i_a \\ i_b \\ i_c \end{bmatrix}; \quad \begin{bmatrix} i_a \\ i_b \\ i_c \end{bmatrix} = \mathbf{C}^{\mathrm{T}}\begin{bmatrix} i_\alpha \\ i_\beta \end{bmatrix} \tag{2}$$

$$\begin{bmatrix} i_d \\ i_q \end{bmatrix} = \mathbf{P}\begin{bmatrix} i_\alpha \\ i_\beta \end{bmatrix}; \quad \begin{bmatrix} i_\alpha \\ i_\beta \end{bmatrix} = \mathbf{P}^{\mathrm{T}}\begin{bmatrix} i_d \\ i_q \end{bmatrix} \tag{3}$$

where $\mathbf{C} = \begin{bmatrix} 1 & -\frac{1}{2} & -\frac{1}{2} \\ 0 & \frac{\sqrt{3}}{2} & -\frac{\sqrt{3}}{2} \end{bmatrix}$; $\mathbf{P} = \begin{bmatrix} \cos\theta & -\sin\theta \\ \sin\theta & \cos\theta \end{bmatrix}$.

Using induction motor as a representative example, a space vector model for this motor is given by:

$$\begin{cases} \vec{v}_s = R_s\vec{\imath}_s + \frac{d}{dt}\vec{\psi}_s; \quad \vec{\psi}_s = L_{ls}\vec{\imath}_s + L_m(\vec{\imath}_s + \vec{\imath}_r) \\ 0 = \vec{v}_r = R_r\vec{\imath}_r + \frac{d}{dt}\vec{\psi}_r; \; \vec{\psi}_r = L_{lr}\vec{\imath}_r + L_m(\vec{\imath}_s + \vec{\imath}_r) \end{cases} \tag{4}$$

where $\vec{v}_s, \vec{\imath}_s, \vec{\psi}_s$ are stator voltage, current and flux linkage, respectively;

$\vec{v}_r, \vec{\imath}_r, \vec{\psi}_r$ are rotor voltage, current and flux linkage, respectively;

$R_s, L_{ls}$ are stator resistance and leakage inductance;

$R_r, L_{lr}$ are rotor resistance and leakage inductance;

$L_m$ is magnetizing inductance.

Other definitions related to the above include:

$L_s = L_m + L_{ls}$ is stator inductance;

$L_r = L_m + L_{lr}$ is rotor inductance;

$\sigma = 1 - \frac{L_m^2}{L_r L_s}$ is leakage constant.

The way the model (4) is utilized in the motor control depends on an adopted control concept. Modern industry currently utilizes two vector control concepts with manufacturer-dependent variations: Field Oriented Control (FOC) and Direct Torque Control (DTC). They are illustrated in Fig.2(a) and Fig.2(b), respectively, and are reviewed below.

### *A. Field Oriented Control (FOC)*

The FOC scheme was first introduced 50 years ago by Blaschke [8]. This scheme is based on a representation of AC quantities in a rotating $dq$-frame that is oriented along one of the flux space vectors. If the $d$-axis of the $dq$-frame is aligned, for example, with $\vec{\psi}_r$, the motor model (4) can be transformed into the following system of equations:

$$\begin{cases} v_{ds} = R_s i_{ds} + \sigma L_s \frac{di_{ds}}{dt} + \left[\frac{L_m}{L_r}\frac{d\psi_r}{dt} - \omega_{syn}\sigma L_s i_{qs}\right] \\ v_{qs} = R_s i_{qs} + \sigma L_s \frac{di_{qs}}{dt} + \left[\omega_{syn}\left(\frac{L_m\psi_r}{L_r} + \sigma L_s i_{ds}\right)\right] \end{cases} \tag{5}$$

$$\frac{d\psi_r}{dt} + \frac{R_r}{L_r}\psi_r = \frac{L_m R_r}{L_r} i_{ds} \tag{6}$$

$$T_{em} = \frac{3}{2}p_p\psi_r\frac{L_m}{L_r}i_{qs}; \qquad \omega_{slip} = \frac{R_r}{L_r}\frac{L_m}{\psi_r}i_{qs} \tag{7}$$

where $\omega_{syn}$ is synchronous frequency;

$\omega_{slip}$ is slip frequency;

$T_{em}$ is electromagnetic torque.

The terms in (5) appearing in square brackets can be separately compensated by feedforward. Ignoring these, equations (5) reduce to two identical linear first order models that are very easy to control. Additionally, as follows from (6) and (7), rotor flux is controlled solely by $i_{ds}$, while torque and slip are controlled solely by $i_{qs}$. This is similar to the effects of, respectively, magnetizing and torque producing currents in DC motors. This similarity, as well as the fact that all AC quantities appear in the synchronously rotating $dq$-frame as DC quantities, turn an AC motor under FOC into a *virtual DC motor*.

*1) Advantages of FOC include:*

- Applicability of Linear Control theory and associated tools (easily tuned PID control, straightforward proof of stability, predictable steady-state and dynamic performance, etc.);
- Consistent performance across the entire range of conditions (including 100% torque at zero speed);
- The use of a Pulse Width Modulator (PWM), with added advantages (predictable harmonic spectrum, easy filter design, low current harmonic distortion owing to that switching harmonics around 10kHz are filtered by motor inductance, etc);

*2) Disadvantages of FOC include:*

- Computational complexity including two angular transformations (although this is acceptable for modern processors);
- Dependence on known motor parameters that change during operation due to heating (although robust and adaptive FOC options are available [11]-[12]);
- The use of speed measurement by a sensor (although speed sensorless FOC options are also available [13]).

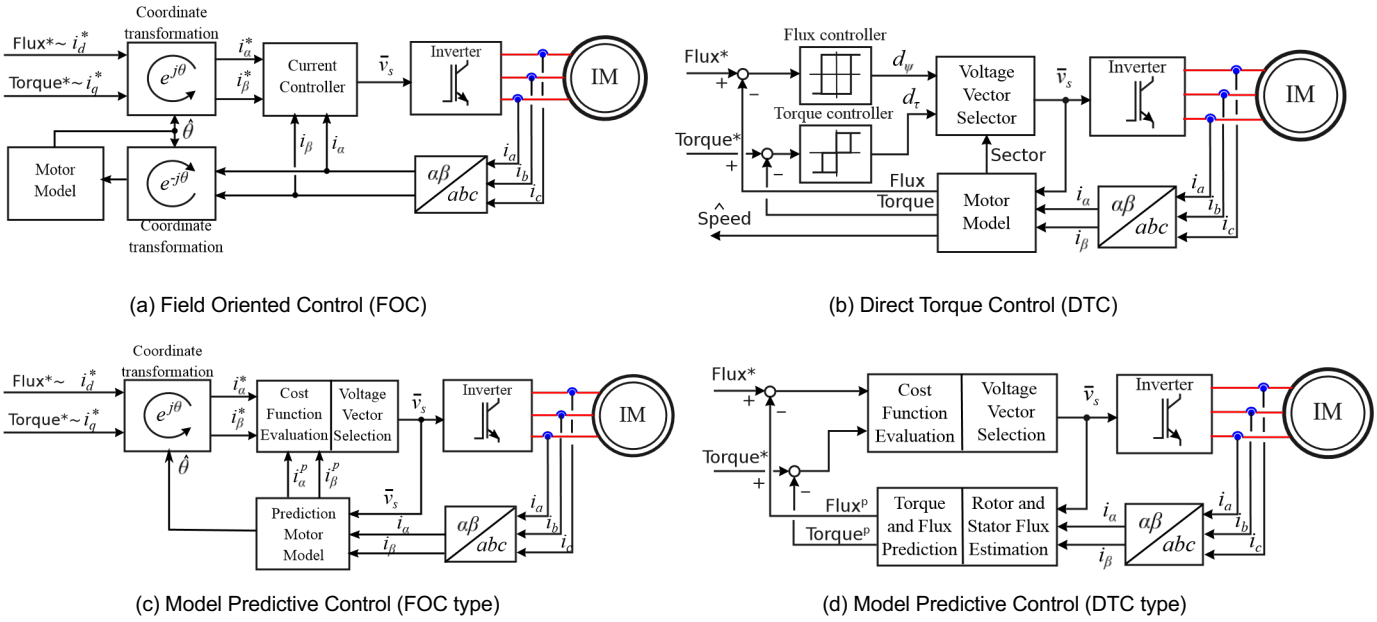


(a) Field Oriented Control (FOC)

(b) Direct Torque Control (DTC)

(c) Model Predictive Control (FOC type)

(d) Model Predictive Control (DTC type)

Fig. 2 Operating principles of various vector control schemes

### *B. Direct Torque Control (DTC)*

The DTC scheme shown in Fig.2(b) was introduced in the 1980s by Depenbrock [9] and Takahashi-Noguchi [10]. The core idea of DTC is based on observation, from voltage equations (4), that the change in stator flux over a control cycle is proportional to the applied stator voltage, or $\Delta\vec{\psi}_s \approx \vec{v}_s T_s$. Additionally, since torque $T_{em} \propto \psi_s \psi_r \sin\theta_{\psi_s\psi_r}$ then changes in both stator flux and torque directly depend on a selected stator voltage in each control cycle. Hence $\vec{v}_s$ can be so selected as to achieve the desired changes in both quantities. The main working formulae are given below.

$$\vec{\psi}_s(T_s) = \vec{\psi}_s(0) + \int_0^{T_s}(\vec{v}_s - R_s\vec{\imath}_s)dt \tag{8}$$

$$\vec{\psi}_r = \frac{L_r}{L_m}\left(\vec{\psi}_s - \sigma L_s\vec{\imath}_s\right); \quad T_{em} = \frac{3}{2}p_p\frac{L_m}{\sigma L_s L_r}\vec{\psi}_r \times \vec{\psi}_s \tag{9}$$

$$T_{em} = \frac{3}{2}p_p\vec{\psi}_s \times \vec{\imath}_s; \qquad \omega_{slip} = \frac{2}{3}\frac{R_r}{p_p L_r}\frac{L_m T_{em}}{\psi_r^2} \tag{10}$$

$$\omega_{syn} = \frac{\theta_{\psi_s}(T_s) - \theta_{\psi_s}(0)}{T_s}; \qquad \hat{\omega}_m = \frac{1}{p_p}(\omega_{syn} - \omega_{slip}) \tag{11}$$

#### *1) Advantages of DTC include:*

- Being amenable to sensorless control: $\omega_m$ measurement can be replaced by $\hat{\omega}_m$ estimation from (11) or observer [14];
- Simplicity of implementation (selection of $\vec{v}_s$ from a lookup table, hysteresis control of $\vec{\psi}_s$ and $T_{em}$);
- Faster dynamic response than with FOC, due to simultaneous adjustments of magnetizing and torque producing currents in desired directions, to increase/decrease torque.

#### *2) Disadvantages of DTC include:*

- Nonlinear dependence of controlled quantities on manipulated variables ($\vec{v}_s$), hence tuning, stability proof, performance expectations, etc. are not straightforward;
- Performance degradation at low speed, due to the effect of $R_s\vec{\imath}_s$ term in (8) (however, this can be addressed [15]);
- Distributed harmonic spectrum, no pronounced switching frequency, hence filter design is challenging (however, options with constant switching frequency are also available [16]).

### *C. Conclusions drawn from FOC and DTC analysis*

From the above review, important conclusions can be drawn in relation to what makes a control solution an industry success.

- Firstly, it is a solid fundamental principle that treats the underlying physical phenomena in a new way (e.g., with DTC: direct manipulation of torque and flux versus current control).
- Secondly, it is a new industry challenge (e.g., with DTC: faster dynamic response that helps reduce an operation cycle and increase productivity).
- Thirdly, it is practical consideration of industrial conditions (e.g., with DTC: removal of a speed sensor from contact with potentially hostile environment).
- Next, it is necessary for a control solution to be robust, i.e. to successfully operate under disturbances, parameter changes and unmodelled nonlinearities.
- Importantly, it needs to appeal to the skill set of industry operators and engineers. In the case of transition FOC→DTC, intuitive tuning of PI current controllers was replaced by intuitive tuning of hysteresis bands of torque and flux controllers.
- Furthermore, electric drives with in-built self-commissioning have become standard.

With the above understanding of the industry success factors, MPC can now be discussed.

## III. MODEL PREDICTIVE CONTROL FOR VSD

The distinctive features of MPC include prediction of a system's future behaviour using its model, evaluation of a cost (or objective) function based on a chosen criteria, and setting

the manipulated input so as to minimize the cost function. In the context of control of power converters, the latter comes down to selection of an optimal switching state from the available Finite Control Set (FCS).

Following the logic of FOC and DTC for electric drives, prediction model and cost function can be formulated with respect to either stator currents, or torque and flux. The two associated classes of MPC schemes, MPC-FOC and MPC-DTC, are illustrated in Fig.2(c) and Fig.2(d), respectively.

### A. Field Oriented MPC (FOC-MPC)

The FOC-MPC option shown in Fig.2(c) can be formulated using the following predictive model. Using Park transform (3) and assuming $\frac{d\psi_r}{dt} = 0$ and $\psi_r = L_m i_{ds} = const$, stator voltage equations (5) can be converted to $\alpha\beta$-frame as follows:

$$\begin{cases} v_{\alpha s} = R_s i_{\alpha s} + \sigma L_s \frac{di_{\alpha s}}{dt} + e_{\alpha s} \\ v_{\beta s} = R_s i_{\beta s} + \sigma L_s \frac{di_{\beta s}}{dt} + e_{\beta s} \end{cases} \quad (12)$$

where $e_{\alpha s} = -\omega_{syn}\psi_r \frac{L_m}{L_r}\sin\theta$ and $e_{\beta s} = \omega_{syn}\psi_r \frac{L_m}{L_r}\cos\theta$ are back-emf projections onto the $\alpha\beta$-axes.

Next, converting model (12) into a discrete form results in the following prediction model (identical for $\alpha$- and $\beta$-currents):

$$i_{s,j}^{p}(k+1) = a i_s(k) + b\left[v_{s,j}(k) - e_s(k)\right] \quad (13)$$

where $a = e^{-\frac{R_s T_s}{\sigma L_s}}$; $b = \frac{1}{R_s}\left(1 - e^{-\frac{R_s T_s}{\sigma L_s}}\right)$;

$i(k)$ is measured stator current at instant $k$;

$v_{s,j}\ (j = 0 \ldots n-1)$ are voltages corresponding to $n$ available switching states of a power converter;

$i_{s,j}^{p}(k+1)$ are stator current predictions at instant $k+1$, provided that voltage $v_{s,j}$ is applied at instant $k$.

If the objective is that current $(i_{\alpha s},\ i_{\beta s})$ follows a given trajectory $(i_{\alpha s}^{*}, i_{\beta s}^{*})$, the following cost function may be used:

$$g_j = \left(i_{\alpha s,j}^{p}(k+1) - i_{\alpha s}^{*}\right)^2 + \left(i_{\beta s,j}^{p}(k+1) - i_{\beta s}^{*}\right)^2 \quad (14)$$

Values of cost function $g_i$, calculated for each voltage from FCS, are then compared. Finally, the voltage $\left(v_{\alpha s}^{opt}, v_{\beta s}^{opt}\right)$ that brings the minimum cost value $g^{min}$ is selected and applied.

### B. Direct Torque MPC (DTC-MPC)

The DTC-MPC option illustrated in Fig.2(d) can be formulated as follows. The full induction motor in model in $\alpha\beta$ -frame (without any assumptions) can be expressed in terms of the state variables $\vec{\psi}_s$ and $\vec{\imath}_s$ as:

$$\begin{cases} \frac{d}{dt}\vec{\psi}_s = A_{11}\cdot\vec{\psi}_s + A_{12}\vec{\imath}_s + B_1\vec{v}_s \\ \frac{d}{dt}\vec{\imath}_s = A_{21}\cdot\vec{\psi}_s - A_{22}\vec{\imath}_s + B_2\vec{v}_s \end{cases} \quad (15)$$

where $A_{11} = 0$; $A_{12} = -R_s$;

$A_{21} = \frac{1}{\sigma L_s}\left(\frac{R_r}{L_r} - jp_p\omega_m\right)$; $A_{22} = -\left(\frac{R_r}{\sigma L_r} + \frac{R_s}{\sigma L_s}\right) + jp_p\omega_m$;

$B_1 = 1$; $B_2 = \frac{1}{\sigma L_s}$;

$\omega_m$ is mechanical (rotor) speed;

$p_p$ is motor pole pair number.

Next, using Euler approximation, a discrete-time model of system (15) can be obtained. Using this model, predicted $\vec{\psi}_{s,j}^{\,p}(k+1)$ and $\vec{\imath}_{s,j}^{\,p}(k+1)$ values can be formed for every $\vec{v}_{s,j}$ from FCS. The corresponding torque predictions are given by:

$$T_{em}^{p}(k+1) = \frac{3}{2}p_p\vec{\psi}_{s,j}^{\,p}(k+1) \times \vec{\imath}_{s,j}^{\,p}(k+1) \quad (16)$$

Cost function for every $\vec{v}_{s,j}$ from FCS can be evaluated from:

$$G_j = \left(\left|\vec{\psi}_{s,j}^{\,p}(k+1)\right| - \psi_s^{*}\right)^2 + \lambda\left(T_{em}^{p}(k+1) - T_{em}^{*}\right)^2 \quad (17)$$

where $\psi_s^{*}$ is the desired average stator flux magnitude;

$T_{em}^{*}$ is the desired average torque;

$\lambda$ is weighting factor to adjust a trade-off between the flux and torque tracking.

Finally, the voltage $\vec{v}_s^{\,opt}\left(v_{\alpha s}^{opt}, v_{\beta s}^{opt}\right)$ that brings the minimum cost value $G^{min}$, is selected and applied.

In the sequel, discussion focuses on the FOC-MPC option.

## IV. MPC CHALLENGES AND ENHANCEMENTS

In the light of the discussion presented in section II, to be successful in industry, MPC is expected to demonstrate:

- High quality reference tracking and dynamic performance;
- Robustness (i.e. immunity to parameter errors, disturbances and other non-ideal conditions) and stability;
- Intuitive tuning and self-commissioning;
- Flexibility and availability of different options: e.g., with harmonics spectrum concentrated at switching frequencies or distributed, with or without common-mode voltage mitigation;
- Consistent and predictable performance across a range of conditions;
- Extra advantages addressing new and emerging challenges.

### A. High Quality Performance Robustness and Stability

An important insight into the existing performance limitations of MPC can be gained by its equivalent representation as follows. First, by inverting model (13) with respect to reference current $i_s^{*}$, reference voltage $v_s^{*}(k)$ can be found as:

$$v_s^{*}(k) = \frac{1}{b}\left(i_s^{*} - a i_s(k)\right) - e_s(k) \quad (18)$$

for $\alpha$- and $\beta$-components. Next, expressing $i_s^{*}$ from (18) and substituting it, along with $i_{s,j}^{\mathrm{p}}(k+1)$ from prediction (13), into the cost function expression (14), yields $g_j = b^2 g_j'$ such that

$$g_i' = \left(v_{\alpha s,j}(k) - v_{\alpha s}^{*}(k)\right)^2 + \left(v_{\beta s,j}(k) - v_{\beta s}^{*}(k)\right)^2 \quad (19)$$

Since the two cost functions relate via a constant coefficient, then the current-based cost function (14) and the voltage-based cost function (19) will be minimized by the same choice of the optimal voltage $v_{s,j}^{opt}$. Hence, they are interchangeable.

The advantage of using the second option is that it allows to split MPC into two distinct parts: "controller" given by (18) and "modulator" given by (19). Clearly, "controller" (18) represents Proportional Control with gain $1/b$, and "modulator" (19) is a

Nearest Neighbor Quantizer (NNQ) that works by choosing the nearest voltage (in the Euclidean distance sense) to the desired voltage $v_s^*(k)$. Current control loop corresponding to this interpretation of MPC is shown in Fig.3(a).

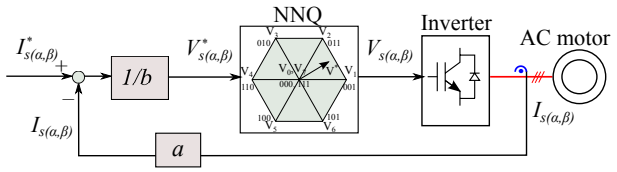


(a) MPC based on the inverse model and NNQ

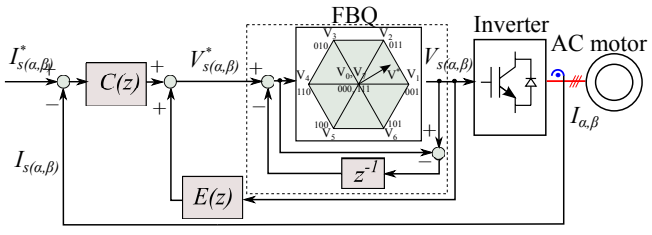


(b) Advanced MPC based on optimal control and FBQ

Fig. 3 Standard and advanced MPC options

Proportional control without integral action is expected to have tracking errors, parameter sensitivity and poor rejection of disturbances, which are the known drawbacks of the standard MPC [17], [4]. NNQ does not guarantee that its output voltage has gain 1 with respect to the reference voltage $v_s^*(k)$. If one wishes to use MPC in high performance applications, then both "controller" and "modulator" need improvements.

***Integral action*** can be achieved by optimal control (in MPC sense) that includes a model for disturbance and is designed to reject it. If current control is performed in the rotating $dq$-frame (where AC quantities appear as DC) then DC disturbance should be rejected. If current control is performed in the stationary $\alpha\beta$-frame then disturbance at the fundamental AC frequency should be rejected.

General framework presented in [18] assists in designing optimal control with integral action in polynomial form. The resulting (improved) control structure is shown in Fig.3(b) where transfer functions $C(z)$ and $E(z)$ are given by (20) if the design is performed in $dq$-frame, and by (21) if the design is performed in $\alpha\beta$-frame.

$$C(z) = K_p^{opt}; \quad E(z) = \frac{(1-a)z^{-1}}{1-az^{-1}} \tag{20}$$

$$C(z) = K_p^{opt} \frac{c_0 - c_1 z^{-1} + az^{-2}}{1 - 2\gamma\cos(\omega_0 T_s)z^{-1} + \gamma^2 z^{-2}}$$
$$E(z) = z^{-1} \frac{e_0 - e_1 z^{-1}}{1 - 2\gamma\cos(\omega_0 T_s)z^{-1} + \gamma^2 z^{-2}} \tag{21}$$

where $K_p^{opt} = 1/b$;

$c_0 = e_0 + a$; $c_1 = e_1 + 2a\cos(\omega_0 T_s)$;

$e_0 = 2(1-\gamma)\cos(\omega_0 T_s)$; $e_1 = (1-\gamma^2)$;

$\gamma$ is the design parameter.

Note that design (20) corresponds to optimal PI control and design (21) - to optimal PR control, with gains defined above as $K_p^{opt}$ and time constants given by $T_i^{opt} = \sigma L_s/R_s$.

Consequently, the advantages of ***intuitive tuning*** (with predictable effect on performance) and ***easy-to-prove stability*** are preserved.

### *B. Flexibility and Availability of Various Options*

An additional effect of splitting MPC into "controller" and "modulator" is that the improved controller can now be combined with different modulators. Commonly used carrier based PWM or Space Vector Modulators (SVM) result in voltages and currents as shown in Fig.4(a), with significant harmonics grouped around $(1,2,\dots) \times f_{sw}$, where $f_{sw}$ is constant and known switching frequency. If such a harmonic spectrum is desirable, then the proposed MPC can use PWM or SVM in its "modulator" stage.

Alternatively, to reduce audible noise and electromagnetic interference (EMI), it can be advantageous to utilize voltages and currents with distributed harmonic spectrum. A high-quality modulator with such a property can be included in the MPC scheme by a simple modification of the previously discussed NNQ. This is shown in Fig.3(b) by a block labelled "FBQ".

***Feedback Quantizer*** (FBQ) includes a feedback loop around NNQ, based on voltage quantization error $q_e(z)$. In the simplest case, this feedback has gain $z^{-1}$. In other words, the quantization error $q_e$ calculated in the previous step, is subtracted from voltage reference $v^*$ in the current step [19]. It can be easily shown that the output (quantized) voltage of the FBQ is then given by

$$v^Q(k)\& = w^*(k) - q_e(k) = v^*(k) - q_e(k-1) + q_e(k) = v^*(z) + S(z)q_e(z) \tag{22}$$

where $S(z) = 1 - z^{-1}$ is noise sensitivity function that shapes the FBQ quantization noise.

Compared to the NNQ output noise $q_e(z)$, the spectrum of the FBQ output noise $S(z)q_e(z)$ is shifted away from the fundamental frequency towards higher frequencies. Also, according to (22), the voltage reference $v^*(z)$ is reproduced at the FBQ output with gain 1.

Additionally, by using a specially designed feedback filter $H(z)$ instead of $z^{-1}$, it is further possible to shape the converter quantization noise in a desired way [19]. The voltage and current produced when using FBQ, as well their harmonic contents, are shown in Fig.4(b). In this case, the feedback filter $H(z)$ is designed to introduce an optional notch at a given frequency (1kHz, in this example). This leads to suppression of mechanical resonances and/or EMI at this frequency.

***Mitigation of Common Mode Voltage (CMV)*** is another useful option that can be included in the MPC suite of options. The root cause of the CMV generation is the fact that the three phase voltages corresponding to the switching states of a VSD are instantaneously unbalanced. This unbalance does not affect the essential motor operation as it averages to zero over a fraction of a fundamental period. However, as a side effect, a high frequency CMV is produced at the motor neutral connection, which tends to form conductive paths through parasitic capacitances.

CMV and the associated current are responsible for several undesirable effects, including damage of motor bearings, the radiated and the conducted EMI, and protection challenges [20]. In mining environment, due to the use of IT earthing system, these issues are further exacerbated. Furthermore, in some cases, ground fault protection may become compromised [21].

To mitigate CMV, control set of a power converter used in a VSD can be restricted by eliminating switching states with high CMV.

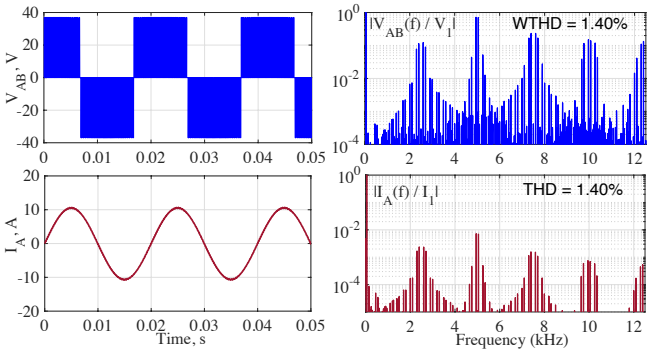


(a) Carrier PWM or SVM: voltage $V_{ab}$, current $I_a$ and their spectra

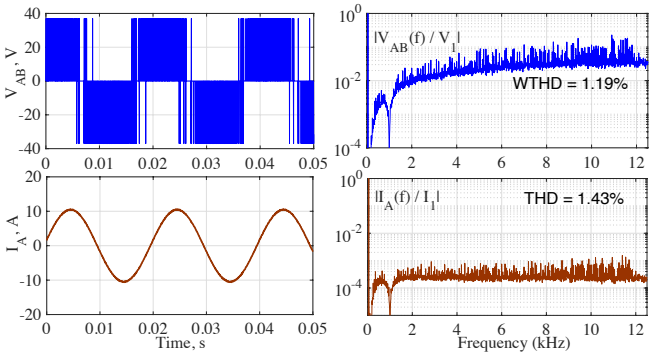


(b) FBQ: voltage $V_{ab}$, current $I_a$ and their spectra (with optional notch)

Fig. 4 Voltage, current and their spectra for different modulators

Some power converter topologies have sufficient redundancy of switching states to completely eliminate CMV. An example of such a power converter is inverter with Active Front End (AFE). CMV mitigation with this topology and the associated trade-offs will be discussed in a case study presented in section V.

### C. Consistency of Performance Across Operating Conditions

One frequently mentioned MPC advantage is its ability to address multiple control objectives of different nature. For example, for an AFE-inverter VSD, it may be desired to:

- minimize tracking errors of the motor side currents;
- minimize harmonic distortion of the AFE side currents;
- minimize the DC-link voltage deviation from a setpoint;
- minimize common-mode voltage at the motor neutral point;
- minimize switching losses of both AFE and inverter.

Under the standard MPC approach, to achieve these multiple objectives, a separate term for each objective is included in the cost function. The total cost function can then be defined as:

$$\begin{aligned} g_{cm}^{total} = {} & \lambda\left[\left(i_{s\alpha,j}^{p}(k)-i_{s\alpha}^{*}\right)^2+\left(i_{s\beta,j}^{p}(k)-i_{s\beta}^{*}\right)^2\right] \\ & +\lambda_f\left[\left(i_{f\alpha,j}^{p}(k)-i_{f\alpha}^{*}\right)^2+\left(i_{f\beta,j}^{p}(k)-i_{f\beta}^{*}\right)^2\right] \\ & +\lambda_{dc}\left(V_{dc,j}^{p}(k)-V_{dc}^{*}\right)^2+\lambda_{cm}\left(V_{cm,j}^{p}\right)^2 \\ & \lambda_{sw,s}\Delta u_s(k)+\lambda_{sw,f}\Delta u_f(k) \end{aligned} \quad (23)$$

where "$s$", "$f$", "$dc$", "$cm$" and "$sw$" denote stator (motor side), filter (AFE side), DC-link, CMV and switching, respectively;

$\lambda_x$ is weighting factor assigned to the term "$x$";

$\Delta u$ is difference between two consecutive switch positions of the corresponding side converter.

Weighting factors $\lambda_x$ in (23) determine trade-offs between the control objectives. Setting them in a reasonable way is crucial for the MPC performance. However, there is no standard procedure or intuitive way to determine $\lambda_x$. Furthermore, depending on operating conditions, the cost terms in (23) may vary relative to each other. Therefore, for consistent performance, weighting factors $\lambda_x$ need to be continuously adjusted.

One way to address this problem is to try minimizing the use of weighting factors altogether. Firstly, redundant terms may be excluded from the cost function. For example, the second term in (23) that penalizes the $i_f$ current error, and the third term that penalizes the $V_{dc}$ error, are related, since closed-loop control on $V_{dc}$ produces the reference $i_f^*$. Therefore, it is sufficient to use the second term in (23) for both measures.

Next, it may be possible to address the remaining (essential) cost terms, architecturally, in different ways. For example, if CMV needs to be restricted to given limits $\pm V_{cm}^{max}$, then all switching states that are charaterised by $|V_{cm}| > V_{cm}^{max}$ should be excluded from the FCS. Penalty on switching, $\Delta u_s$ and $\Delta u_f$, can be addressed by considering the previous switching state and excluding from the FCS the prospective switching combinations that lead to changes of more than $N$ switches at once. Alternatively, switching transitions can be interpreted in terms of Euclidean distances using Voronoi Diagrams [22], so that a single cost term can be used to penalize for both tracking error and switching.

As a result, the cost function for AFE-inverter can be reduced to include only two terms. Using the equivalence of the current-based (14) and the voltage-based (19) cost functions leads to

$$\begin{aligned} g_{cm}^{total} = {} & b_s^2\lambda\left[\left(i_{s\alpha,j}^{p}(k)-i_{s\alpha}^{*}\right)^2+\left(i_{s\beta,j}^{p}(k)-i_{s\beta}^{*}\right)^2\right] \\ & +b_f^2\left[\left(i_{f\alpha,j}^{p}(k)-i_{f\alpha}^{*}\right)^2+\left(i_{f\beta,j}^{p}(k)-i_{f\beta}^{*}\right)^2\right] \end{aligned} \quad (24)$$

where $\lambda$ is a single weighting factor that determines the trade-off between the motor and the AFE current quality;

$$b_s = \frac{1}{R_s}\left(1-e^{-\frac{R_s T_s}{\sigma L_s}}\right) \approx \frac{T_s}{\sigma L_s};$$

$$b_f = \frac{1}{R_f}\left(1-e^{-\frac{R_f T_s}{L_f}}\right) \approx \frac{T_s}{L_f}.$$

The value of $\lambda$, as a function of operating conditions, can be determined from first principles (e.g., power balance), as will be demonstrated in section V. Then a practical and consistent weighting of the control objectives will be maintained.

### D. Extra Advantages to Address New Industry Challenges

This relates to finding an answer to a reasonable question: "what can MPC offer that the existing schemes, e.g., FOC and DTC, cannot?" An answer to this question may be found by considering modern power converter topologies that have been recently introduced to the VSD market and have brought new control challenges. One specific example is that of a matrix converter, that offers a dramatic reduction of a VSD size and weight by eliminating the DC-link capacitor stage [5].

Its control by standard methods is difficult due to a tight coupling between input and output, nonlinear dynamics and under-actuation, while the MPC concept is naturally fitting. Matrix converter control is discussed in a companion paper.

## V. SIMULATION AND EXPERIMENTAL RESULTS

The ideas presented in section IV have been validated by simulation and experiment. As a case study, a VSD with Active Front End (AFE) driving a 10kW 4-pole 415V induction motor, was selected. The environment emulated in this study corresponds to an underground mining application, where it is common to use IT earthing system with a neutral-to-earth resistor (NER). A typical NER value is $150\Omega$. Fig.5(a) shows the VSD structure and connection diagram including a transformer.

Fig.5(a) also shows a closed path for the common-mode current via NER. The common-mode current containing high-frequency switching noise creates a notable voltage drop ($V_{NER}$) on the NER, which adds to all three phase voltages at the transformer output. This causes a conducted EMI affecting all devices connected to the same transformer. This undesirable effect can be mitigated by eliminating its root cause – the CMV.

The experimental equipment used in this study is detailed in Fig.5(b). The test induction motor is mechanically loaded by a DC motor on a test bed. The inverter and the AFE are based on standard industrial IGBT stacks. The control software is customized and uploaded to the drive from a computer.

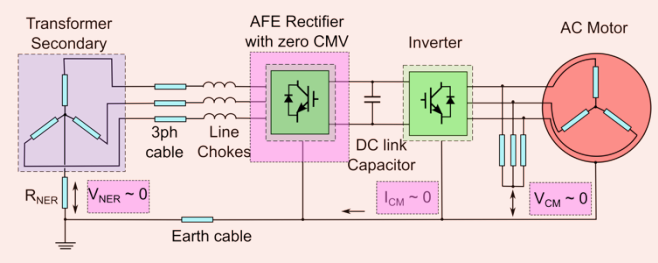


(a) Variable Speed Drive based on an inverter with AFE

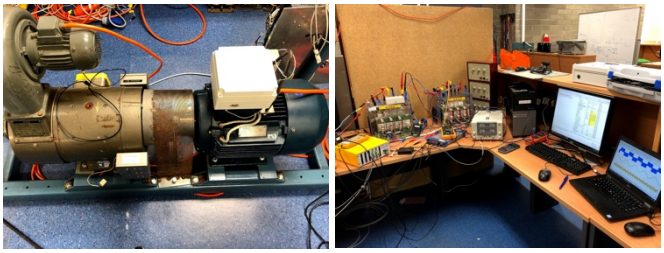

(b) Test (right) and load (left) motors, inverter, AFE and control system

Fig. 5 Experimental VSD: (a) structure, (b) physical equipment

Parameters used in the simulations matched the experimental parameters. These were, for the motor: $R_s = R_r = 0.3\Omega$, $L_m = 100mH$, $L_{ls} = L_{lr} = 5mH$. The input filter for AFE had: $R_i = 0.4\Omega$, $L_i = 5mH$. Three VSD control options were considered in both simulations and experiments: the standard MPC (as per Fig.3(a)), the advanced FBQ-MPC (as per Fig.3(b)), and the advanced FBQ-MPC with CMV elimination.

Simulation results shown in Fig.6 compare transient operation under the three schemes. The motor was accelerated to its rated speed, then at $t = 0.5s$ the load increased by $10\,\text{Nm}$ and at $t = 0.7s$ the motor was commanded to stop. Dynamic performance in all three cases looks similar. However, FBQ-MPC (see Fig.6(b)) produces much smaller current distortion and torque ripple than the standard MPC (see Fig.6(a)). The last option (Fig.6(c)) has similar torque ripple to the standard MPC but completely eliminates the CMV.

Fig.7 presents a zoomed view of constant speed operation, corresponding to the time interval $0.55\ldots0.6s$ in Fig.6. The details of the relevant mechanical and electrical quantities can be clearly observed. Under FBQ-MPC with CMV elimination, the voltage waveform is more irregular than under the two other options. This is due to the restriction on the control set.

Fig.8 presents steady-state experimental results for the three control options. The AFE-side current distortion under the standard MPC is higher than in the corresponding simulation. Under FBQ-MPC with the CMV elimination, a low-level noise is observed in the CMV, as compared to a perfect zero in simulation. This can be explained by an unavoidable effect of the switching delays due to dead-time.

Both simulation and experimental results demonstrate advantages of the advanced FBQ-MPC compared to the standard MPC. Degradation of the current quality when the CMV elimination option is selected, is unavoidable but not significant.

Transient plots presented in Fig.6 assist in selection of the weighting factor $\lambda$ to be used in the cost function (24). Using the torque expression (7) and given that $i_{ds} = const$, the motor-side current dependency on torque can be obtained as:

$$i_s^2 = i_{ds}^2 + i_{qs}^2 = i_{ds}^2 + \frac{T_{em}^2}{K_T^2 i_{ds}^2} \approx \frac{T_{em}^2}{K_T^2 i_{ds}^2} = \frac{P_m^2}{\omega_m^2 K_T^2 i_{ds}^2} \qquad (25)$$

where $k_T = \frac{3}{2} p_p \frac{L_m^2}{L_r}$.

The AFE-side (grid) voltage $v_g$ is constant, while the AFE is controlled to maintain its input current $\vec{\imath}_f$ at unity power factor with the grid voltage vector $\vec{v}_g$. Hence, the input current magnitude $i_f$ is proportional to power $P_{in}$ supplied from grid. Ignoring losses makes $P_{in} \approx P_m$, hence $i_f^2 \propto P_m^2$.

Say that a suitable trade-off between the AFE and the motor side currents can be established under one given speed $\omega_1$, resulting in a certain choice, $\lambda_1$. Then, to maintain consistency of the performance trade-offs for an arbitrary speed $\omega_m$, the weighting factor $\lambda$ in (24) can be determined as $\lambda_1 \omega_m^2 / \omega_1^2$.

## VI. CONCLUSIONS

This paper has presented a review of control strategies used by the industry in VSD applications. It has formulated a list of expectations for a new control strategy to be an industry success. From that viewpoint, the paper has critically evaluated MPC and its features, and identified areas of improvement.

The paper has proposed several important modifications to the standard MPC, to close the gaps between the existing and the expected performance. The proposed modifications have been validated by simulation and experiment under steady-state and transient conditions.

The proposed advancements are shown to overcome the existing barriers in MPC applications to industry, and offer clear benefits for demanding industrial environments, such as mining. New and emerging trends in power converter technology will take a further advantage of the MPC, in its best forms.

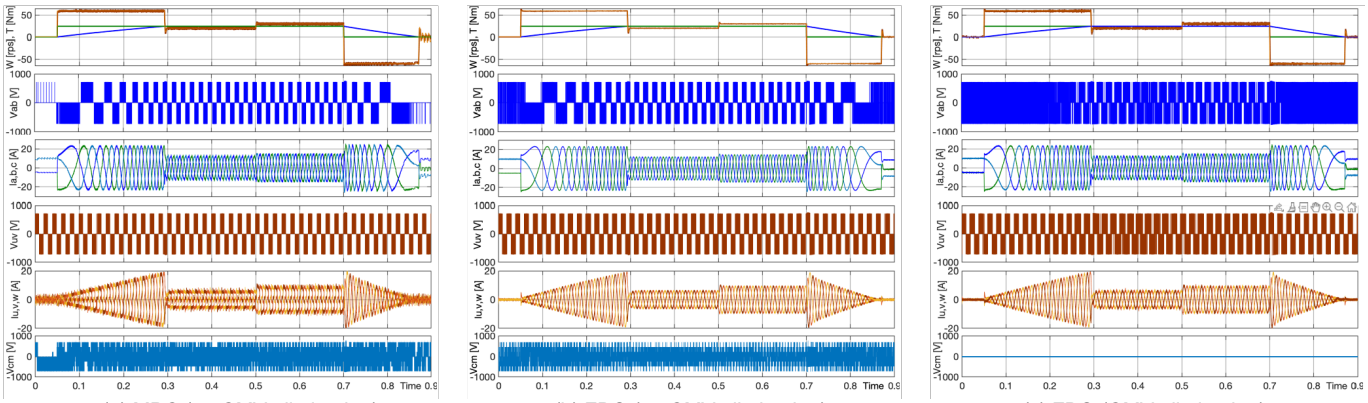

(a) MPC (no CMV elimination) (b) FBQ (no CMV elimination) (c) FBQ (CMV elimination)

Fig. 6 Transient simulations: 1) motor speed $\omega_m$ vs $\omega_m^*$ and torque $T_{em}$ vs $T_{em}^*$; 2) motor-side line-to-line voltage $V_{ab}$; 3) motor-side line currents $I_a, I_b, I_c$; 4) grid-side line-to-line voltage $V_{uv}$; 5) grid-side line currents $I_u, I_v, I_w$; 6) common-mode voltage $V_{cm}$.

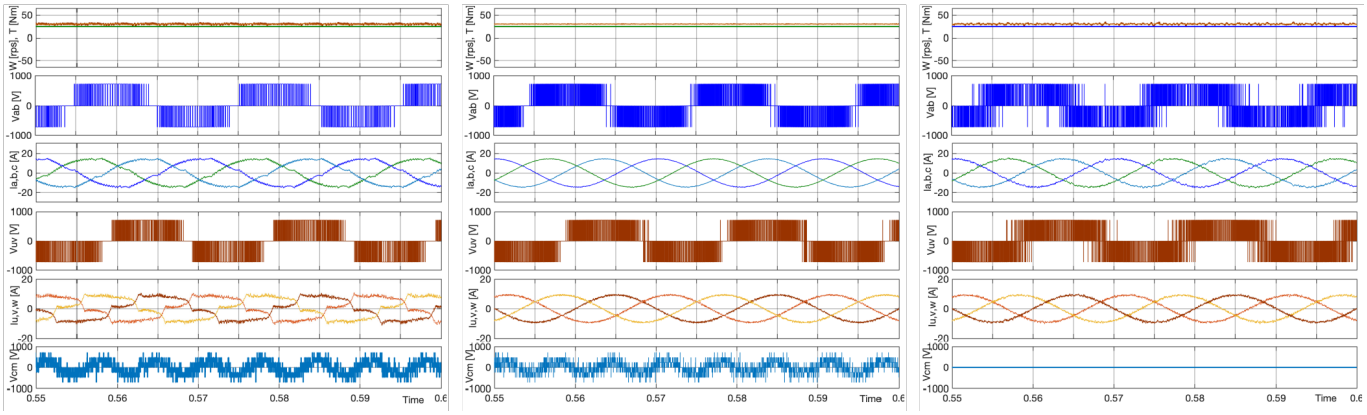

(a) MPC (no CMV elimination) (b) FBQ (no CMV elimination) (c) FBQ (CMV elimination)

Fig. 7 Steady-state simulations: 1) motor speed $\omega_m$ vs $\omega_m^*$ and torque $T_{em}$ vs $T_{em}^*$; 2) motor-side line-to-line voltage $V_{ab}$; 3) motor-side line currents $I_a, I_b, I_c$; 4) grid-side line-to-line voltage $V_{uv}$; 5) grid-side line currents $I_u, I_v, I_w$; 6) common-mode voltage $V_{cm}$.

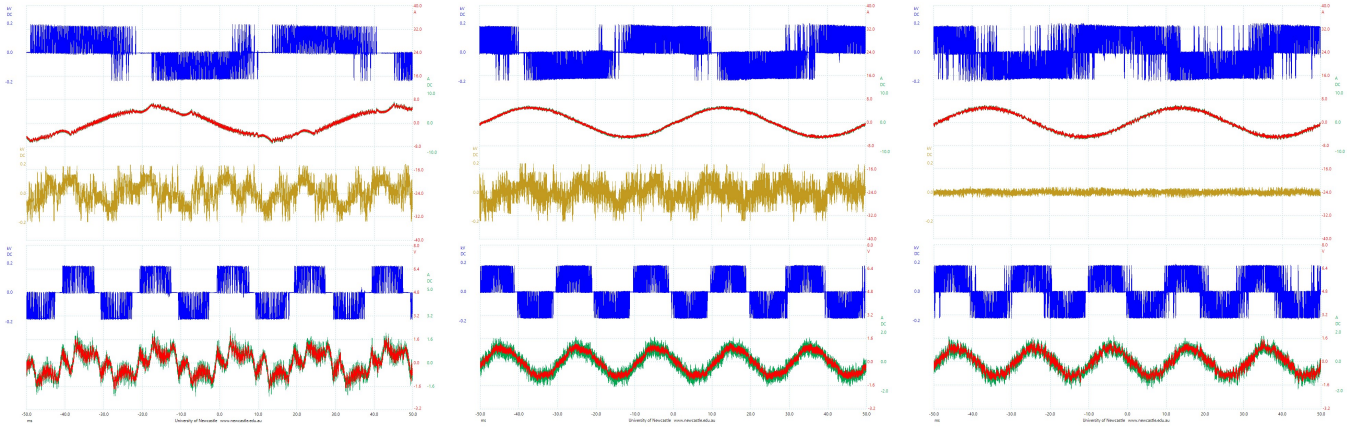

(a) MPC (no CMV elimination) (b) FBQ (no CMV elimination) (c) FBQ (CMV elimination)

Fig. 8 Experimental results for the AFE-VSD: motor-side line-to-line voltage $V_{ab}$; motor-side line current$I_a$; common-mode voltage $V_{cm}$; grid-side line-to-line voltage $V_{uv}$; grid-side line current $I_u$.

## VII. REFERENCES


[1] J. B. Rawlings and D. Q. Mayne, *Model Predictive Control: Theory and Design*. Madison, WI, USA:Nob Hill, 2009.

[2] A. Linder and R. Kennel, "Model predictive control for electrical drives," in *2005 IEEE 36th Power Electronics Specialists Conference Record*, 2005, pp. 1793–1799.

[3] J. Rodriguez and P. Cortes, *Predictive control of power converters and electrical drives*, vol. 40. John Wiley & Sons, 2012.

[4] M. Norambuena, P. Lezana, and J. Rodriguez, "A method to eliminate steady state error of model predictive control in power electronics," *IEEE Journal of Emerging and Selected Topics in Power Electronics*, vol 7, pp 2525-2530, Dec 2019.

[5] J. Lei, S. Feng, P. Wheeler, B. Zhou, and J. Zhao, "Steady-state error suppression and simplified implementation of direct source current control for matrix converter with model predictive control," *IEEE Transactions on Power Electronics*, vol 35, pp 3183-3194, Mar 2020.

[6] T. J. Besselmann, S. Van de Moortel, S. Almer, P. Jorg, and H. J. Ferreau, "Model predictive control in the multi-megawatt range," *IEEE Transactions on Industrial Electronics*, vol 63, pp 4641-4648, Jul 2016.

[7] V. Spudic and T. Geyer, "Model predictive control based on optimized pulse patterns for modular multilevel converter STATCOM," *IEEE Transactions on Industry Applications*, vol 55, pp 6137-6149, Nov/Dec 2019.

[8] F. Blaschke, "The principle of field-orientation as applied to the new TRANSVEKTOR closed-loop control system for rotating-field machines," *Siemens Review*, vol. 34, pp. 217–220, 1972.

[9] M. Depenbrock, "Direct self-control (DSC) of inverter-fed induction machine," *IEEE Transactions on Power Electronics*, vol 3, pp 420-429, Oct 1988.

[10] I. Takahashi and T. Noguchi, "A new quick-response and high-efficiency control strategy of an induction motor," *IEEE Transactions on Industry Applications*, vol IA-22, pp 820-827, Sep 1986.

[11] S. Khadar, H. Abu-Rub, and A. Kouzou, "Sensorless field-oriented control for open-end winding five-phase induction motor with parameters estimation," *IEEE Open Journal of the Industrial Electronics Society*, vol. 2, pp. 266–279, 2021.

[12] S. Yang, D. Ding, X. Li, Z. Xie, X. Zhang, and L. Chang, "A novel online parameter estimation method for indirect field oriented induction motor drives," *IEEE Transactions on Energy Conversion*, vol 32, pp 1562-1573, Dec 2017.

[13] J. Holtz, "Sensorless control of induction machines - with or without signal injection?," *IEEE Transactions on Industrial Electronics*, vol 53, pp 7-30, Feb 2006.

[14] T. R. Tesch and R. D. Lorenz, "Disturbance torque and motion state estimation using low resolution position interfaces," *in IEEE 41st IAS Annual Meeting Conference Record*, 2006, pp 917-924.

[15] Y. Xu, Y. Wang, R. Iida, and R. D. Lorenz, "Extending low-speed self-sensing via flux tracking with volt-second sensing," *IEEE Transactions on Industry Applications*, vol 54, pp 4405-4414, Sep/Oct 2018.

[16] N. Idris and A. Yatim, "Direct torque control of induction machines with constant switching frequency and reduced torque ripple," *IEEE Transactions on Industrial Electronics*, vol 51, pp 758-767, Aug 2004.

[17] R. P. Aguilera, P. Lezana, and D. E. Quevedo, "Finite-control-set model predictive control with improved steady-state performance," *IEEE Transactions on Industrial Informatics*, vol 9, pp 658-667, May 2013.

[18] G. Mirzaeva, G.C. Goodwin, B.P. McGrath, C. Texeira, and M.E. Rivera, "A generalized MPC framework for the design and comparison of VSI current controllers," *IEEE Transactions on Industrial Electronics*, vol 63, pp 5816-5826, Sep 2016.

[19] G. Mirzaeva and G. Goodwin, "The use of feedback quantizer PWM for shaping inverter noise spectrum," in *15th EPE/PEMC Conference Record*, 2012, pp 960-966.

[20] J. Luszcz, "Modeling of common mode currents induced by motor cable in converter fed ac motor drives," in *IEEE ISEMC Conference Record*, 2011, pp. 459–464.

[21] G. Mirzaeva, D. Carter, S. M. M. Uddin, and P. Stepien, "Common mode voltage elimination in variable speed drives for improved electrical safety," *IEEE Transactions on Industry Applications*, vol 56, pp 4365-4374, Jul/Aug 2020.

[22] G. Mirzaeva, G. Goodwin, and C. Townsend, "A simple and effective strategy to reduce switching losses under fs-MPC based on dynamically changing Voronoi diagrams," in *12th IEEE ICIEA Conference Record, 2017*, pp. 1516–1521.


## VIII. VITAE

Galina Mirzaeva received BEng degree in electronic engineering in 1990 and PhD in electrical engineering in 1997 from the South Urals State University, Russia.

From 2004 to 2010, she worked at CRC-Mining, Australia. Since 2010, she has been with the School of Engineering at the University of Newcastle, Australia, first as Senior Lecturer and from 2017 - as Associate Professor.

Her research interests include power electronics, electric drives, renewable energy integration and electric transportation. Dr Mirzaeva currently serves as Chair of the IEEE IAS Mining Industry Committee.

Yunxun Mo received BEng degree in electrical engineering from Harbin Institute of Technology, China in 2019. In 2021, he received master's degree in electrical engineering at University of New South Wales, Sydney, Australia.

His research interests include power electronics, microgrids, electric transportation and renewable energy integration. Mr. Mo currently studying at University of Newcastle in his first year of PhD program.